

Research Papers



Experimental investigation of the impact of mechanical deformation on aging, safety and electrical behavior of 18650 lithium-ion battery cells

Markus Spielbauer^{a,b,*}, Jonas Soellner^b, Philipp Berg^b, Korbinian Koch^{b,c}, Peter Keil^d, Christian Rosenmüller^a, Oliver Bohlen^a, Andreas Jossen^b

^a Department of Electrical Engineering and Information Technology, Munich University of Applied Sciences, Lothstr. 64, 80335 Munich, Germany

^b Technical University of Munich, School of Engineering and Design, Department of Energy and Process Engineering, Chair of Electrical Energy Storage Technology, Arcisstr. 21, 80333 Munich, Germany

^c TÜV SÜD Battery Testing GmbH, Daimlerstr. 15, 85748 Garching, Germany

^d Battery Dynamics GmbH, Battery Dynamics GmbH, Lichtenbergstr. 8, 85748 Garching, Germany

ARTICLE INFO

Keywords:

18650 lithium-ion battery
Mechanical abuse test
Deformation
Long-term aging
Safety

ABSTRACT

Particularly in mobile applications, 18650 lithium-ion batteries can be exposed to mechanical abuse. Deforming mechanical abuse can severely damage the battery case, but sometimes without causing instantaneous cell failure. If such cases remain undetected, the cells may remain in use and pose a potential long-term safety hazard. Due to research gaps in the scientific literature regarding the long-term implications of such damage, the influence of cell design, intrusion depth, as well as the impact on the electrical behavior, two cyclic aging studies and further electrical tests (CC–CV capacity, DVA) were conducted with mechanically deformed 18650 cells; using CT, post-mortem, and SEM for further analysis. In the cyclic aging studies, both cell types tested (with a mandrel and mandrel-free) remained electrically functional and showed no safety-critical behavior, despite intrusions of up to 6 mm. Cells with significant intrusion exhibited increased CC–CV charge capacity for one charging process, and CC-discharge capacity decreases of 3.2% after mechanical deformation, but no or only slightly accelerated aging rates after the initial capacity drop. DVA indicated a global capacity loss of useable material rather than specific anode or cathode damage. CT analysis revealed case re-deformation after cyclic aging, likely due to jelly roll swelling. Post-mortem analysis showed imprints on all electrode components and active material debonding. SEM analysis revealed changes in cell internal pressure distribution due to external deformation.

1. Introduction

Lithium-ion batteries are utilized in various mobile applications, such as power tools, mobile devices, and electric vehicles. A critical issue for lithium-ion batteries is the safety aspect, originating in the properties of the components, which some of are flammable (anode active material, electrolyte solvents), oxygen-containing (cathode active material), and toxic (conducting salt). With an increasing number of systems in use and rising energy densities, the amount and severity of hazardous incidents [1–5] may increase further. To prevent such incidents, significant effort is made to detect them before their occurrence, to mitigate their impact by different means [4,6–8] and improve our understanding of the causes and mechanisms for the optimization of cell and pack design. One of the causes of hazardous events, to which cells in mobile applications may be exposed in particular, is deforming mechanical abuse.

Even in normal operating conditions, mechanical forces are omnipresent in lithium-ion batteries at the cell, electrode, and particle levels and are interdependent with the cyclic aging behavior. At the cell level, the main mechanisms causing electrochemical–mechanical interactions are breathing and swelling. Breathing refers to lithiation-induced reversible cyclic volume changes of the cathode and, especially, of the anode active materials (up to 10% in the thickness direction) [9–12] during charge and discharge cycles. Swelling refers to progressive increases in thickness due to aging-related side reactions, boundary layer growth, plating [13–15], and a corresponding rise in cell-internal stress. To avoid the breathing-induced delamination of electrode layers, pouch and prismatic cells are often braced. However, excessive bracing pressure must be avoided as well, as this can also reduce cell lifespan [16–20]. Also, in cylindrical cells, these forces play

* Corresponding author at: Department of Electrical Engineering and Information Technology, Munich University of Applied Sciences, Lothstr. 64, 80335 Munich, Germany.

E-mail address: markus.spielbauer@hm.edu (M. Spielbauer).

<https://doi.org/10.1016/j.est.2022.105564>

Received 4 June 2022; Received in revised form 22 August 2022; Accepted 26 August 2022

Available online 19 September 2022

2352-152X/© 2022 The Authors. Published by Elsevier Ltd. This is an open access article under the CC BY license (<http://creativecommons.org/licenses/by/4.0/>).

a significant role, as mechanical jelly roll collapsing is considered a crucial factor in cyclic aging [21,22].

At the electrode level, stress gradients can occur at local imperfections, such as the current collector tabs. These can lead to an inhomogeneous electrode and separator compression and cause inhomogeneous charge transfer and electric characteristics. Such local defects may cause inhomogeneous aging and increase the risk of local lithium plating [23–28]. Some researchers argue that such local defects could also cause dendrite growth through the separator and ISCs in lithium-ion batteries, analogous to lithium-metal batteries [24]. Additionally, breathing-induced repeated loading and unloading of the separator in high-pressure areas may result in fatigue.

At the particle level, the active material expansion leads to microscopic effects, since intercalation of lithium causes stress within particles, and external stress causes inhomogeneous intercalation. Cyclic expansion and shrinking, in combination with inhomogeneous intercalation between [29] and in particles [30–32], can cause progressive mechanical failure of the binder. Additionally, this can result in cracking and breaking down of the particles, thereby causing a loss of active material alongside the consumption of electrolyte and cyclable lithium at newly formed boundary layers. With increasing shares of silicon in the anode active material to enhance the energy density, which exhibits significantly more mechanical expansion during charge [33,34], the relevance of these issues will likely further increase.

In the case of external deforming mechanical abuse, these cell-extrinsic mechanical forces interact with the cell-intrinsic, potentially causing increased pressure levels and inhomogeneity. The immediate effect of external mechanical abuse on cells has been analyzed in various publications with various form factors, types, geometries, chemistries, and abuse conditions [35–42]. Also, the immediate influences of SOC [43] and SOH [43–45] on the behavior of lithium-ion batteries under mechanical abuse have been investigated.

However, mechanical deformation may also occur without immediately causing hazardous events. If such deformation remains undetected, the damaged cells may remain in use and pose a potential long-term safety hazard. Potential causes for delayed failure include excessive cell-internal pressure due to cell-external deformation and a corresponding increased risk of plating, dendrite growth, and separator fatigue [46]. Additionally, non-hazardous impairments of functionality may occur, such as increased inhomogeneity of current distributions on the module level [47,48], which may accelerate aging. On the other hand, if it turns out that such scenarios do not degrade battery safety, this might allow weight savings in module design due to reduced safety requirements. Potential application scenarios are, for example, power tool or e-bike batteries that might be dropped from a significant height, thereby causing reversible elastic deformation of the battery pack casing and permanent plastic deformation of the batteries themselves; or else, in automotive applications, impacts of road debris in a battery pack in automotive applications [49].

While cyclic aging under normal operating conditions has been investigated in-depth in scientific literature [50–53], studies investigating the potential long-term implications of mechanical loads and deformations on the safety and cyclic aging behavior of lithium-ion batteries are scarce, with an overview over the available literature given subsequently.

Kim et al. [54] applied bending and torsion to lithium-polymer pouch cells. They observed limited impact on the capacity during cyclic aging up to 50 cycles from bending up to 15°, while torsion tests lead to accelerated aging, especially for the maximum of 15°. Fuchs et al. [27] applied deformation to a pouch cell with a steel ball with 4 mm diameter, and compared the results between a cycled and an uncycled deformed cell in a post-mortem and SEM analysis. Zhu et al. [55] investigated the impact of indentation with various impactors on the electrical behavior of small format pouch cells (5 cycles) and conducted EIS, CT, SEM, and post-mortem analysis. Goodman et al. [56] conducted a long-term aging test series (1000 cycles) with

small-format pouch cells damaged by three-point bending. Applying electrical characterization, CT, and post-mortem analysis, they reported that, despite the occurrence of ISCs, many cells remained electrically functional but showed accelerated aging behavior.

For 18 650 lithium-ion batteries, Shuai et al. [57] applied flat compression with various indentation depths up to 5 mm and conducted OCV measurements, pulse discharge tests, and capacity measurements for parameter identification for circuit models. They reported that deformed cells were still useable but exhibited significant capacity drops. However, they did not investigate long-term cycling. Sahraei et al. [58] applied rod indentation with a diameter of 6 mm up to an indentation depth of 4.6 mm to 18 650 LFP batteries and cycled them at different C-Rates up to 89 times. They reported no significant difference between the indented and intact cells. Soudbakhsh et al. [59] from the same research group published an article with rod deformation with a diameter 15.8 mm up to 5 mm intrusion, analyzing the impact on EIS and fitting parameters of an equivalent circuit model. They reported only a minor influence from mechanical deformation in initial capacities. Li et al. [60] applied flat radial compression with 3 and 6 mm intrusion to 21 700 cells, cycled the cells for 100 cycles, and characterized them with incremental capacity analysis (ICA), EIS and CT. They reported significantly accelerated aging for the deformed cells, which might be caused by micro-leakage at the gasket of the positive pole.

While these publications offer a first insight into the electrical behavior and safety of damaged 18 650 cells in short-term cycling scenarios, their results are partly equivocal and expose several gaps in available scientific publications regarding:

- Indentation depth: The influence of indentation depth has not been investigated systematically, and no cells with indentation depth > 5 mm have been cycled so far.
- Cycling duration: No long-term cyclic aging experiments with more than 89 full cycles have been conducted so far.
- Cell design: The influence of cell internal design parameters (e.g. mandrel) has not been investigated.
- Analysis: Implications of mechanical deformation on cyclic aging of 18 650 cells have not yet been analyzed with commonly used methods for battery characterization such as CT, post-mortem and SEM analysis.
- Electrical behavior: Further investigation of electrical behavior (e.g. DVA) may improve the understanding of underlying damage mechanisms or offer approaches for the detection of mechanical damages.

To address these research gaps, this paper presents long-term cyclic aging studies with two types of commercial 18 650 cells with mechanical indentation alongside with the application of common analysis methods and further investigation of their electrical behavior.

2. Experimental

The following section presents the test setups used for the cyclic aging test series and the further electrical tests.

2.1. Cyclic aging test studies

Two cyclic aging studies were conducted on two cell types with the same experimental test setup elaborated in the latter. An overview of the test conditions is given in Table 1.

2.1.1. Cell types

In this work, two types of high-power 18 650 lithium-ion batteries (Samsung INR18 650-25R M, production code SDIEM TH04; Sony/Murata US18 650 VTC5, production code Z119D) were used. From an applicant's perspective, these cells are similar, as they have similar capacities and can provide high discharge currents (as shown

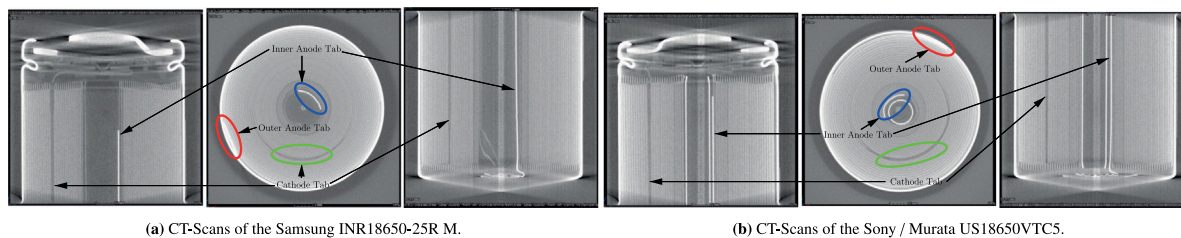


Fig. 1. CT-Scans of the Samsung INR18650-25R M and the Sony/Murata US18650VTC5. Each left column: Axial cross-section of positive pole regions. Middle column: Radial cross-section of the center of the cells. Right column: Axial cross-section of to bottom part of the cells.

Table 1

Overview over conducted cycling aging studies with mechanically damaged cells.

Test series	I	II
Cell type	Samsung INR18650-25R M	Sony/Murata US18650VTC5
Cycling charge	CC-CV 4 A, 0.1 A	
Cycling discharge	CC 10 A	
Rest phase duration	20 min	
Test end criterion	70% SOH or 600 cycles	
Battery tester	Scienlab SL6/30/0.18BTS20C	
Climate chamber	ATT Discovery DM340	
Ambient condition	Temperature chamber, 25 °C, convection box	
Cell contacting	Cell holder with spring probe pins	
Deformation tool	Universal testing machine Test GmbH 112.50 kN H	
Feed rate	0.1 mm s ⁻¹	
Feed hold time	60 s	
Impactor	Cylindric: Ø 20 mm	
Indentation depth	0 mm (reference), 2 mm, 4 mm, 6 mm	
Tab alignment	Inner	
Cells per variation	5	

Table 2

Data sheet specifications of cell types used in this publication.

	Samsung INR18650-25R M [61]	Sony/Murata US18650VTC5 [62]
Nom. discharge capacity	2500 mAh	2600 mAh
Max. cont. discharge	20 A ^a	30 A/20 A ^b
Max. cont. charge current	4 A	4 A
Discharge cut-off voltage	2.5 V	2.0 V

^a60% after 250 cycles.

^b30 A with 80 °C cutoff.

in Table 2). That makes them suitable for many mobile high-power applications and potentially exposed to mechanical damages.

Regarding their mechanical structure, both cells have one cathode current collector tab within the jelly roll and two anode current collector tabs, each at the inner and outer end of the jelly roll, as depicted in Figs. 1(a) and 1(b). A significant mechanical difference between the cells is that the Samsung INR18650-25R M has no mandrel in the center, while the Sony/Murata US18650VTC5 does. Consequently, the jelly roll of the Samsung INR18650-25R M has more space to compensate for deformation by reshaping, while the Sony/Murata US18650VTC5 has less space available. Therefore, it was assumed that this might result in higher cell internal stress and harm the cell safety in long-term cyclic aging studies after deformation.

2.1.2. Test procedure

The same test procedure was chosen for both cyclic aging series, using five cells for each variation. Rather than applying mechanical deformation before starting the long-term cycling tests, the cells were pre-cycled for ten cycles to ensure the finalization of cell formation processes, such as the initial SEI formation [63]. Additionally, this allowed the direct comparison of pre- and post-deformation measurements. CT checkups were conducted at the start of the test series (to mark the tab alignment), after the deformation, and at the end of the long-term

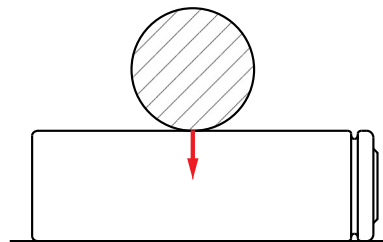


Fig. 2. Deformation setup for the aging studies and electrical investigations.

cyclic aging studies. The cells were analyzed further in post-mortem examination and SEM.

2.1.3. Cell deformation

The deformation of the cells was conducted with a Universal testing machine 112.50 kN H (Test GmbH) with a maximum force of 50 kN, distance measurement with a resolution of 1 μm and a force sensor with class 0.5 according to ISO 7500-1. For the tests, path controlled feed of 0.1 mm s⁻¹ was applied until the desired indentation depth was reached, which was then held for 60 s. To preclude thermal events during the cell deformation, it was conducted at 0% SOC.

During the deformation procedure, the cell temperature was measured with Pt1000 sensors to detect potential heat generation due to ISCs. As the focus of these aging series was on the deformation of the jelly roll, the cells were deformed radially in the cell center with a cylindric impactor with 20 mm diameter, as depicted in Fig. 2, with 2, 4 and 6 mm intrusion. Under the same test conditions in a preceding test series, 50 pristine Samsung INR1860-25R M cells with 0% SOC showed internal short circuits (voltage drop > 2.5 %) at a mean intrusion of 8.05 mm ($\sigma = 0.20$ mm).

2.1.4. Electrical and environmental test conditions

Cyclic aging test series were performed with a cell testing system SL6/30/0.18BTS20C (Scienlab) with a voltage precision of ±1 mV and a current precision of 0.05 % ±25 mA.

For both cyclic aging test series, CC-CV charging with 4 A and 0.1 A cut-off for the CV-phase and CC discharge with 10 A were chosen within a voltage range from 2.5 V to 4.2 V. These test conditions were chosen to represent high load scenarios, as it was assumed that they cause high cell internal mechanical stress. Current limits were set by the data sheets for the charge and the specified temperature operating conditions for the discharge phases. 20 min pauses were applied after each charge and discharge phase for the homogenization of the charge distribution within the electrodes and particles as well as for temperature cooldown. As test end criteria, 70% SOH, as commonly used for cyclic aging series [50–53], or 600 cycles were chosen.

The tests were performed in an ATT Discovery DM340 temperature chamber, equipped with gas sensors and an exhaust system, with a temperature of 25 °C. As the ventilation causes inhomogeneous temperature boundary conditions within the temperature chamber due to different convective heat transfer, the cells were positioned within

polymer boxes, which increased the maximum cell temperature but ensured equal environment conditions for all cells. The cells were contacted using self-constructed cell holders with spring contact pins for four-terminal sensing (two power pins and one sense pin per pole).

2.1.5. Computed tomography analysis

CT scans were conducted with a phoenix nanotom s research|edition (GESensing & Inspection Technologies) with 120 kV voltage, 130 mA current, 2×2 binning, and 1000 images per scan.

2.2. Further electrical tests

To avoid interference of electrical characterization methods with the cyclic aging studies, which might have influenced the electrical behavior directly after the deformation and can cause capacity recovery [64], checkups were not conducted during the long-term test series. Instead, further characterization before and after cell deformation was performed on a separate set of cells.

While some of the commonly used methods for the characterization, such as EIS [59,65], have already been applied to damaged 18 650 cells, others have not. In this work, capacity analysis, open circuit voltage measurements, and differential voltage analysis were conducted.

2.3. Capacity analysis

Capacity and charge curve analyses were conducted for the charge and discharge measurements during the long-term cyclic aging studies. Furthermore, the influence of the charge and discharge direction was investigated on a separate set of cells.

2.3.1. Open circuit voltage measurements and differential voltage analysis

Open circuit voltage measurements and differential voltage analysis may help to understand if deformation inflicts function loss mainly to the anode or cathode. For these tests, a HRT-M5 series tester from Battery Dynamics was used, as it offers significantly higher current (0.05 mA) and voltage precisions ($4 \mu\text{V}$).

OCV measurements were conducted on Samsung INR18 650-25R M cells with CC-CV for charging and discharging in 10 pre-cycles before and after mechanical deformation. For the cycling, C/5 was applied in this case [50,66–70]. For the mechanical deformation, the same settings were chosen as in Table 1 with 2, 4, and 6 mm indentation depth but with deformation at 50% SOC instead. The measurement data was logged with a sampling frequency of 0.1 Hz.

3. Results

After the description of the experimental test setups in the previous section, the following section presents the results of the conducted measurements.

3.1. Results of the aging test series

For the test series with deformation and cyclic aging, CT, post-mortem, and SEM analysis were performed.

3.1.1. Deformation and cyclic aging

For cyclic aging study I, the force–displacement curve (depicted in Fig. 3(a)) during deformation showed more than 8 kN peak load for the cells with 6 mm deformation and significant mechanical relaxation during the 60 s holding phase.

During the long-term cyclic aging of aging study I, none of the deformed cells exhibited any indicators of safety-relevant issues. The averaged discharge capacity curves are depicted in Fig. 3(b). While the deformation seems to have little impact on the CC discharge capacity for cells with 2 mm deformation, cells with 4 mm show small and cells with 6 mm deformation show distinct drops of the discharge capacity

(ca. 0.08 Ah or 3.2 %) after deformation. After this initial drop, the aging of the damaged cells occurred at similar rates as the reference cells.

For cyclic aging study II, the force–displacement curve (depicted in Fig. 3(c)) during deformation showed slightly higher peak loads of more than 9 kN for the cells with 6 mm deformation.

During the long-term cyclic aging of aging study II, none of the deformed cells exhibited any indicators of safety-critical behavior either. Similar to the first aging study, the CC discharge capacities in Fig. 3(d) show significant capacity drops of around 0.08 Ah for the cells with 6 mm intrusion. Regarding the behavior during long-term cyclic aging, the Sony/Murata US18 650VTC5 exhibited a slightly longer life span under the chosen test conditions than the Samsung INR18 650-25R M in the aging study I. While cells with 2 mm and 4 mm deformation showed, apart from initial capacity drops after deformation, no significant increase in the aging rates, the cells with 6 mm deformation showed slightly accelerated aging after 300 cycles.

3.1.2. CT analysis

To analyze the combined effects of mechanical deformation and cyclic aging on the internal structure of the battery cells, CT conducted after the deformation and at the end of the cyclic aging test series are elaborated subsequently.

The CT images of cells of aging study I after the deformation (depicted in Fig. 4(a)) show that increased deformation leads to increasing filling of the void space in the center of the jelly roll. Additionally, active material and separator compression, buckling, delamination, and current collector tab deformation can be observed. Despite the high intrusion, no fracture of the electrode current collectors occurred.

At the end of the aging test series, the reference cells showed mechanical jelly roll collapsing originating from the mechanical inhomogeneity at the cathode current collector tabs, which is typical for cylindrical cells [21,22,71–73]. For the cells with 2 mm deformation, similar mechanical collapsing is also observable, but originating from the external indentation spot instead. For the cells with 4 mm deformation, the collapsing emanates from both the collector tab and the deformation spot. For the cells with 6 mm deformation, no jelly-roll collapsing is visible in this cross-section as there is no space remaining in the cell center. Nevertheless, the cross-sections without direct deformation range still show similar mechanical collapsing.

A comparison of cell thicknesses in the strongest deformed cross-section (Table 3a), shows that due to the elastic deformation of the cells and the universal testing machine, the actual remaining cell deformation is below the applied machine feed. At the end of the aging test series, the cell diameters have increased significantly (0.73 mm for 6 mm indentation).

The CT scans for aging study II, depicted in Fig. 4(b), show that the mandrel poses some resistance to mechanical deformation, but collapses at increased intrusion depths; thus resulting in only minor differences in the effective jelly-roll layer compression. Also for this cell type, no fracture of the electrode current collectors was observable.

At the end of the aging test series, the CT scans of the reference cells show that void spaces in the mandrel region have slightly decreased due to jelly-roll swelling. In this region, minor mechanical collapsing occurred. For the deformed cells, no mechanical collapsing is noticeable in CT cross-sections with the highest deformation, but outside of the indentation zone, mechanical collapsing occurs as well. For the cells with 4 mm and 6 mm deformation, it is noticeable that the impactor-averted side shows significant delamination at the end of the aging test series. Near the mandrel, these cells exhibit some delamination after the end of the aging studies.

The increase of cell diameter (0.95 mm for 6 mm indentation) during the long-term cycling (shown in Table 3b), is slightly higher than in aging test series I, also considering the aging series cells with 2 and 4 mm deformation ended at 600 cycles and not at SOH 70%.

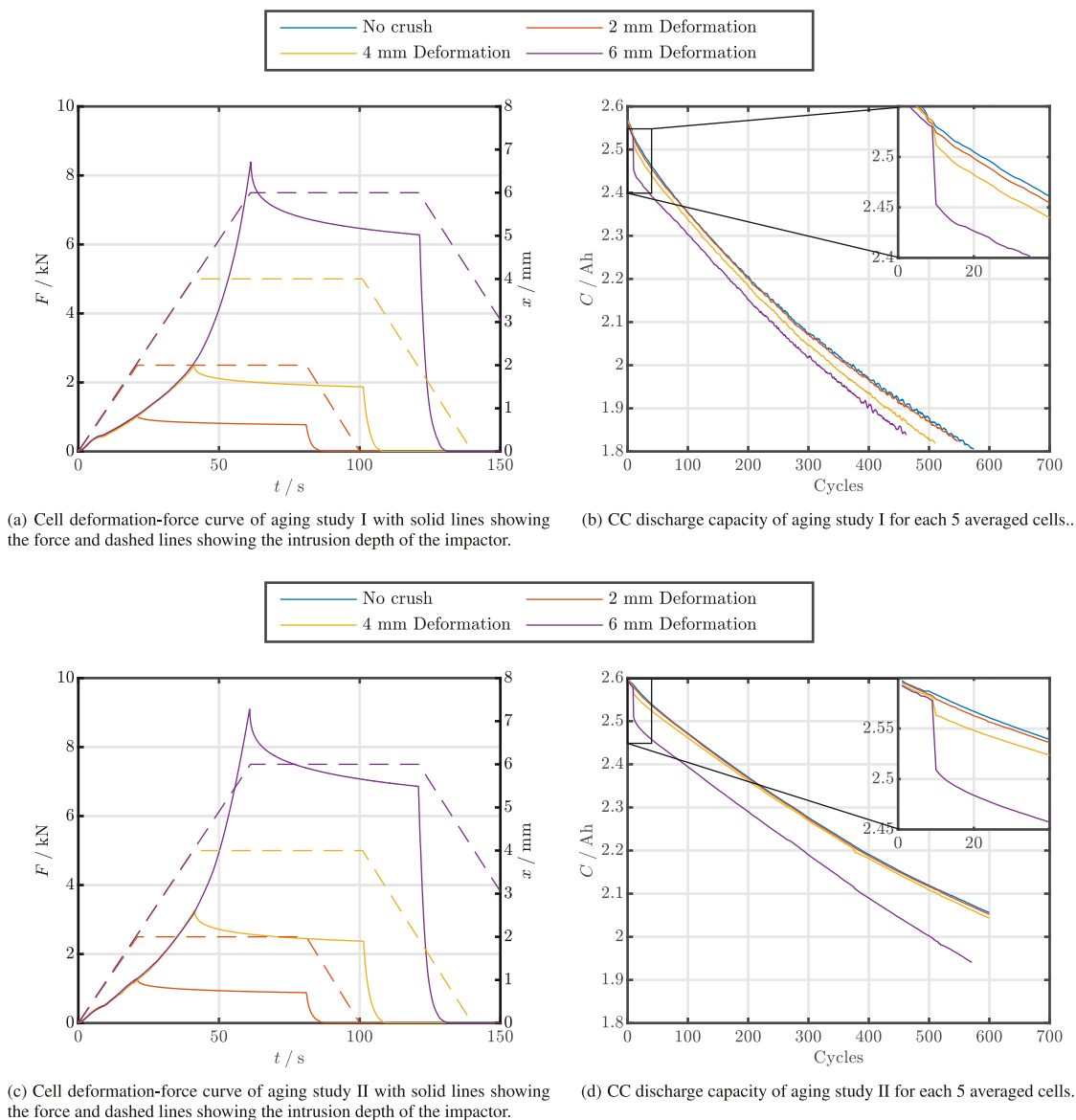


Fig. 3. Cell deformation and discharge capacity fade for both cyclic aging studies of mechanically damaged cells (top: Samsung INR18650-25R M, bottom: Sony/Murata US18650VTC5).

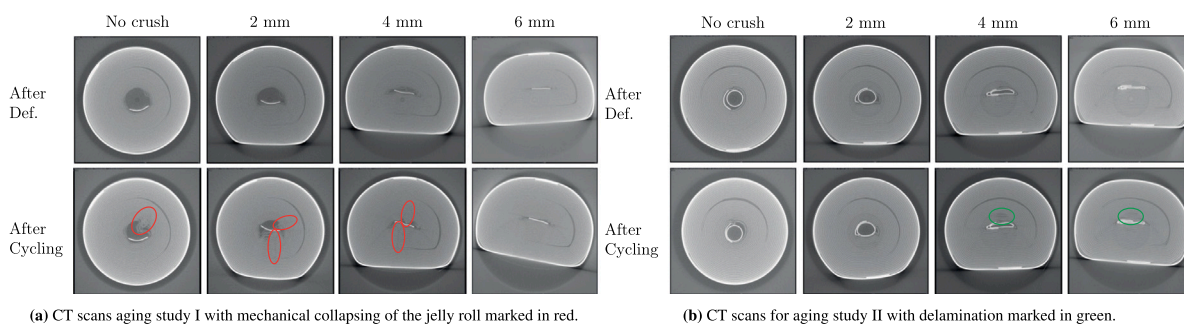


Fig. 4. CT scans in the cross-section of the maximum deformation conducted after cell deformation and after test ending for both aging series.

Table 3

Measurements of the diameter in the deformation cross-section for both cyclic aging studies conducted after deformation and after cycling showing significant jelly roll swelling and re-deformation of the case. The diameter was measured in the cross section with the highest deformation.

(a) Measurement of the diameter in the deformation cross-section for aging study I.				
	Reference	2 mm Def.	4 mm Def.	6 mm Def.
After Def.	18.11 mm	16.72 mm	14.83 mm	13.08 mm
After cycling	18.11 mm	17.09 mm	15.44 mm	13.81 mm
Swelling	0 mm	0.37 mm	0.61 mm	0.73 mm
(b) Measurement of the diameter in the deformation cross-section for aging study II.				
	Reference	2 mm Def.	4 mm Def.	6 mm Def.
After Def.	17.99 mm	16.66 mm	14.84 mm	13.03 mm
After cycling	17.99 mm	17.16 mm	15.47 mm	13.98 mm
Swelling	0 mm	0.50 mm	0.63 mm	0.95 mm

3.1.3. Post-mortem analysis

Post-mortem analysis with cell disassembly and visual inspection of each jelly roll component was conducted at the end of the cyclic aging studies on one cell for each indentation depth. For this, the outward-oriented sides for the anode, cathode, and separators for both the inner and the outer jelly roll areas were analyzed.

The analysis for cyclic aging test series I in Fig. 5(a) shows imprints of the current collectors on the electrodes and separators of the reference cells. In the outer jelly roll area, the cathode shows discoloration patterns at the axial center. In the inner jelly roll area, the electrodes were significantly bent and broke during unrolling. The cathode showed two discoloration bands. With increasing intrusion, the deformed cells show progressively distinct imprints of the impactor with increasing indentation depth on all jelly-roll components and delamination in the impact areas, which is also observable on the opposing electrode surfaces. On the cathode, the discoloration pattern shows significant differences. In the inner jelly roll area, increased delamination after unrolling and axial gaps in all jelly roll layers are observable. Despite these local differences, a significant proportion of the electrodes appears to be unaffected by the mechanical compression.

The analysis of the aging test study II, depicted in Fig. 5(b), likewise shows imprints of the current collectors for the reference cells and discoloration in the outer jelly roll area. Unlike the Samsung INR1865-25R M, for the Sony/Murata US18650VTC5, the inner jelly roll area is easily bendable and unrollable without breaking. For the deformed cells, different coloration patterns are recognizable in both the inner and outer jelly roll areas. In the direct deformation and bending area, patterns with active material debonding can be found on all jelly roll components.

3.1.4. SEM analysis

To investigate if external compression influences the electrode microstructure after cycling, SEM analysis was conducted by Fraunhofer ISC on an aged Samsung INR18650-25R M cell with 4 mm deformation and a cycled reference cell. For the deformed cell, one sample was taken from the outer jelly roll of the non-deformed area and one from the outer jelly roll of the impact area. For comparison with an undeformed cell, samples from a reference cell were taken from the inner and the outer jelly roll area.

The anode of the deformed cell exhibits significant morphology changes, densification, and a lower porosity in the impact area compared to the non-deformed sample in Fig. 6(a). While these differences appear severe, significant gradients can also be observed between the inner and the outer jelly roll of the reference cell Fig. 6(b), even though the densification does not appear to be as severe. For the cathode, the difference between the impact area and the non-deformed area at the outer jelly roll is less significant, as depicted in Fig. 6(c). Also, the visual differences between inner and outer jelly roll are slighter, as shown in Fig. 6(d). In all cathode samples, cracks in particles can be observed.

3.2. Electrical behavior

Regarding the electrical behavior of cells under mechanical indentation, the effects on charge and discharge capacity and DVA are elaborated in the latter.

3.2.1. Capacity behavior

As so far, only the CC-discharge capacity has been analyzed Fig. 7(a) shows the coulombic efficiency for all tested cells for the first 25 cycles of cyclic aging study I (with cyclic aging study II showing similar results). The cells with 4 and 6 mm deformation exhibit severe drops in coulombic efficiency down to 78% in the cycle directly after mechanical deformation.

Further analysis of the charge and discharge capacity, exemplarily depicted in Fig. 7(b) for a cell with 6 mm deformation, reveals that the cause of this behavior is not only the drop in discharge capacity but also a substantial spike of charged capacity in the first cycle after deformation from 2.55 Ah to 2.82 Ah for a cell with 6 mm indentation. That is more than 10% above the specified capacity of the cell type. After this spike in charge capacity, in the following cycle the capacity dropped below the level before the deformation of 2.45 Ah.

The voltage-charging curve in Fig. 7(c) shows that the deformation has only a minor influence on the duration of the CV-phases, whereas the CV-phases are significantly prolonged and show higher charging currents. Further tests indicate that this effect occurs not only in the charge direction but also when cells are deformed at 100% SOC, and then CC-CV discharged. Also, a prolonged CV phase occurs but with significantly smaller charge throughput in the CV phase.

3.2.2. OCV measurements and DVA

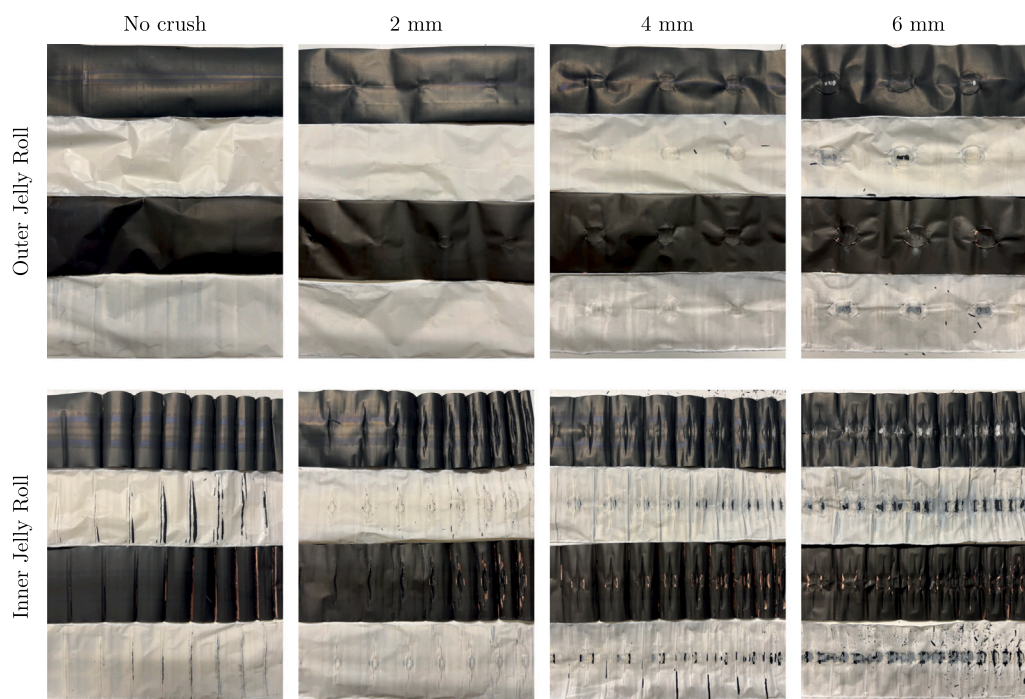
DVA was conducted on the fifth cycle of the OCV measurements before and after the mechanical deformation. The results showed that the reference cells exhibit only marginal shifts in the DVA, which is why they are not presented. The deformed cells show qualitatively similar changes in the DVA, which is why only the variation with the most significant changes (6 mm deformation) is shown.

The DVA over the capacity in Fig. 8(a) for the deformed cell shows the total loss of discharge capacity and the resulting shrinkage of the entire measurement curve. The DVA over the SOH in Fig. 8(b) illustrates no characteristic shifts in the peaks observable for both anode and cathode. Instead, compression of the measurement curve occurs.

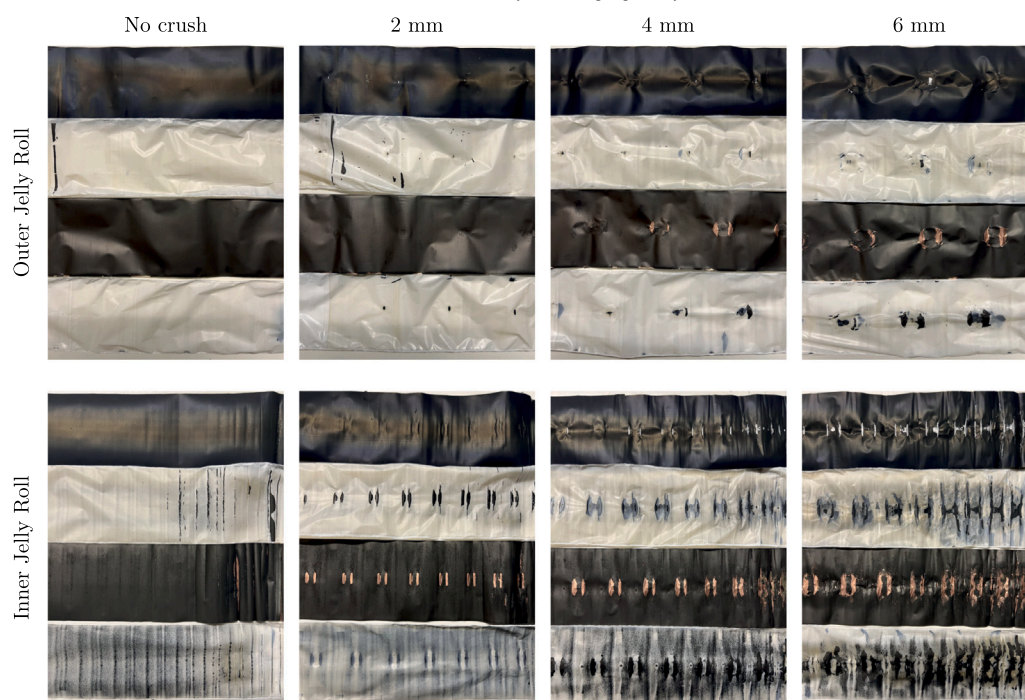
4. Discussion

After elaborating on the measurement results, the following section discusses these findings concerning the identified research gaps. Also, the influence of cell design with CT, post-mortem, and SEM analysis, as well as the electrical behavior are discussed.

Regarding the safety aspect, both cyclic aging test series conducted showed that even severe deformations depths with up to 6 mm intrusion



(a) Post-mortem analysis for aging study I.



(b) Post-mortem analysis for aging study II.

Fig. 5. Post-mortem analysis for both aging studies after test ending showing the outward oriented sides of cathode, separator, anode and separator for both the outer and the inner jelly roll area.

did not cause any hazardous events. Furthermore, even in an aging study of a Samsung INR18 650-25R M cell with electrode fracture with 7.5 mm deformation, which was not elaborated in this publication, the cell was cyclable up until 70% SOH without safety-relevant issues. The postulated scenarios of progressive separator fatigue due to increased swelling forces, breathing, or dendrite growth was not observed.

Regarding the influence of the cell design, the CT analysis shows minor jelly roll collapsing for the reference cells with a mandrel. The higher stiffness of the Sony/Murata US18 650 VTC5 during deformation

could, among other factors such as different material composition and mechanical strength of other components, partly be caused by its presence. The flexible design of the mandrel might be a safety feature, as a rigid mandrel could increase cell-internal stress in the case of deformation, reducing the indentation depth of the onset of an ISC.

Apart from insights regarding the influence of the cell design, the CT analysis also revealed that external mechanical deformation does not cause destruction of the jelly roll structure but primarily reshaping. Additionally, it was observable that external deformation

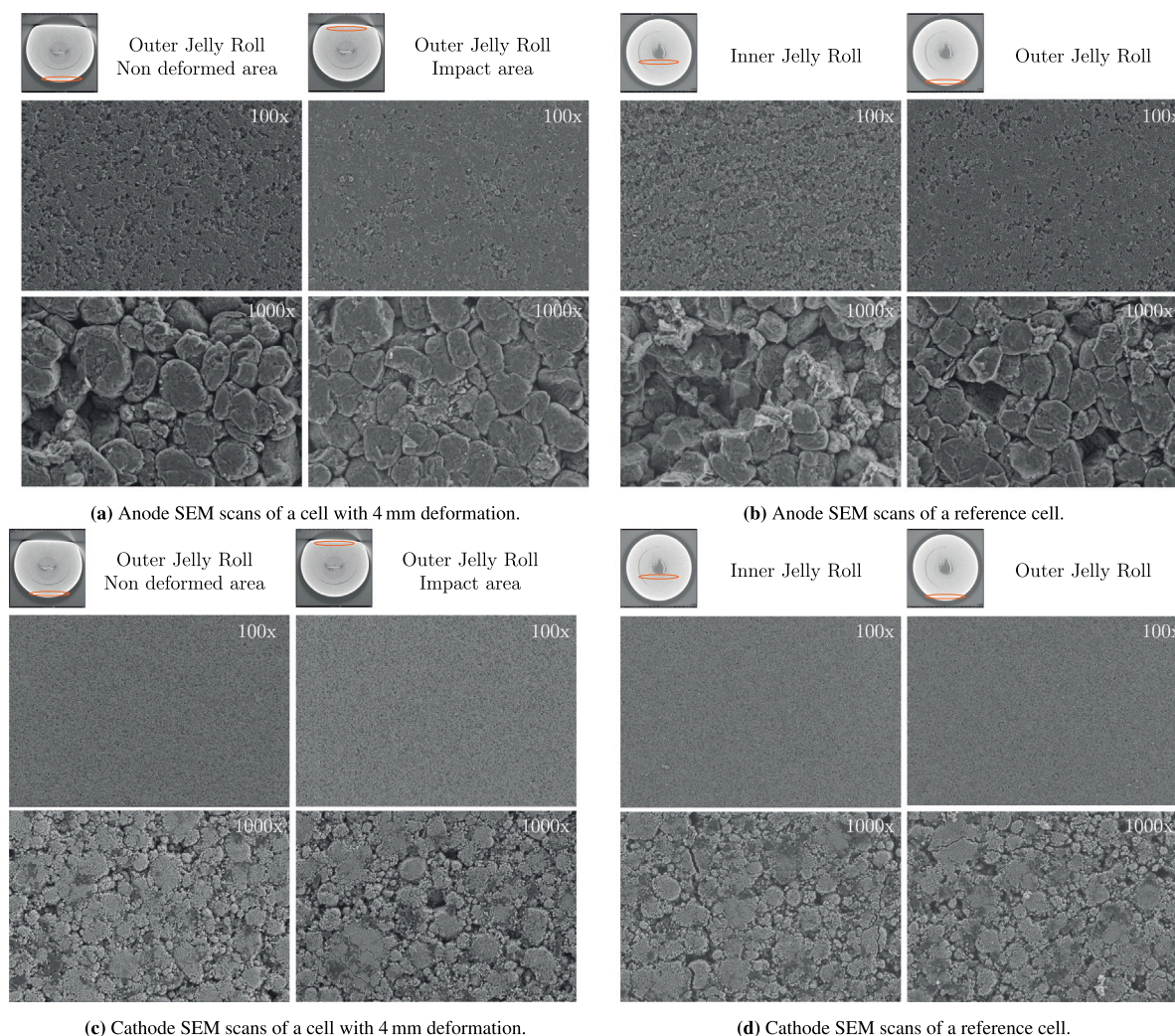


Fig. 6. SEM images of a Samsung INR18 650-25R M cell with 4 mm deformation and a reference with 70% SOH. In the CT scans at the top, the location of the sample extraction is marked in orange. (For interpretation of the references to color in this figure legend, the reader is referred to the web version of this article.)

causes the mechanical collapsing to originate from the external defect rather than cell-internal imperfections. Thickness measurements showed cell diameter increases at the end of the cyclic aging studies for the deformed cells. These increases likely are caused by cell internal pressure increases due to swelling, which partly are compensated by the re-deformation of the cell cases. Delamination for the Sony/Murata US18 650VTC5 with 6 mm deformation may explain increased aging rates.

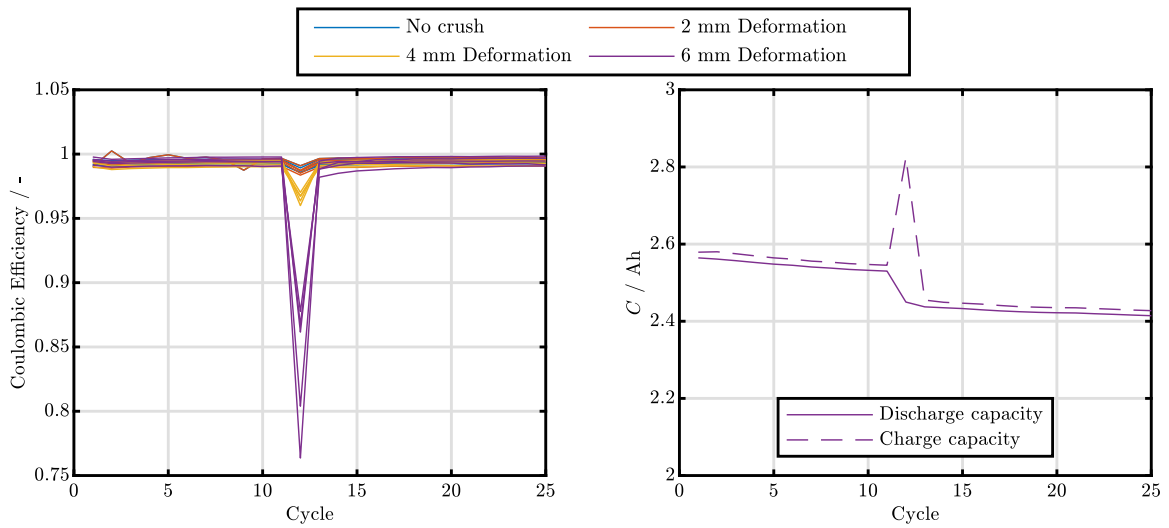
The post-mortem analysis showed active material debonding during unrolling and different cathode discoloration patterns for the deformed cells. Debonding may be caused by excessive mechanical stress that causes the fracture of the active material-current collector interface [75], or can be caused by electrolyte drying out in these regions due to porosity decreases and electrolyte displacement. While the cause for the discoloration remains unclear, it potentially is linked to mechanical stress, with different stress distributions causing different discoloration patterns. Despite severe local defects, large parts of the electrodes remained intact. The separators showed pressure imprints but no signs of fracture or fatigue, which testifies against the presence of an ISC.

The SEM analysis revealed that cell-external pressure may cause significant porosity gradients of the anode, while the cathode exhibited only minor differences in general. Combined with the significant debonding of aged samples of anode active material and its lower mechanical strength in compressive tests [76–80], this may indicate

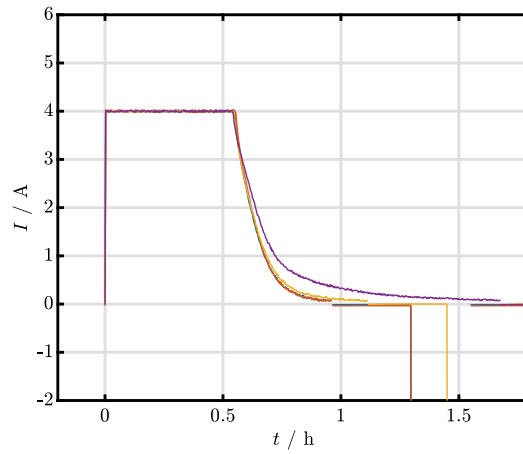
that the anode active material is more susceptible to mechanical stress. However, as porosity gradients can also be found in undeformed reference cells, the deformation may primarily change the pressure distribution within the cell. Excessive stress levels can be expected in the buckling zones, where sample extraction was impossible due to active material debonding during cell disassembling. With this, it has to be considered that SEM images show only a local sample of the electrodes and allow no general statement regarding its entirety.

Regarding the electrical behavior, 6 mm indentation caused discharge capacity drops of 3.2 % after the deformation. After initial drops, the deformed cells showed no or only slightly accelerated aging rates compared to the reference cells during long-term cyclic aging. Such capacity drops are undesirable as they may significantly increase inhomogeneity within a module and cause accelerated aging for the entire system.

Nevertheless, in combination with the increased CC–CV charge capacity directly after deformation (10% for the Samsung INR18 650-25R M) this may offer an approach for damage detection. The low-current cut-off of the CV phases supports the assumption of actual capacity loss rather than resistance increase alone. Significantly smaller charge throughput in the CV phase in the case of discharging may be explained by the steeper OCV curve or by being mainly caused by anode side reactions. Mechanisms causing the initial increase of charged capacity and the subsequent drop of discharge capacity may be cracking and pulverization of active material, as well as the formation of new SEI and



(a) Coulombic efficiency after deformation for all 5 cells of each variation. (b) Charge and discharge capacity of a cell with 6 mm deformation.



(c) Prolonged CV-phases during cell charge in the cycle right after cell deformation.

Fig. 7. Electrical behavior of damaged battery cells during charging after mechanical deformation of cells of aging study I.

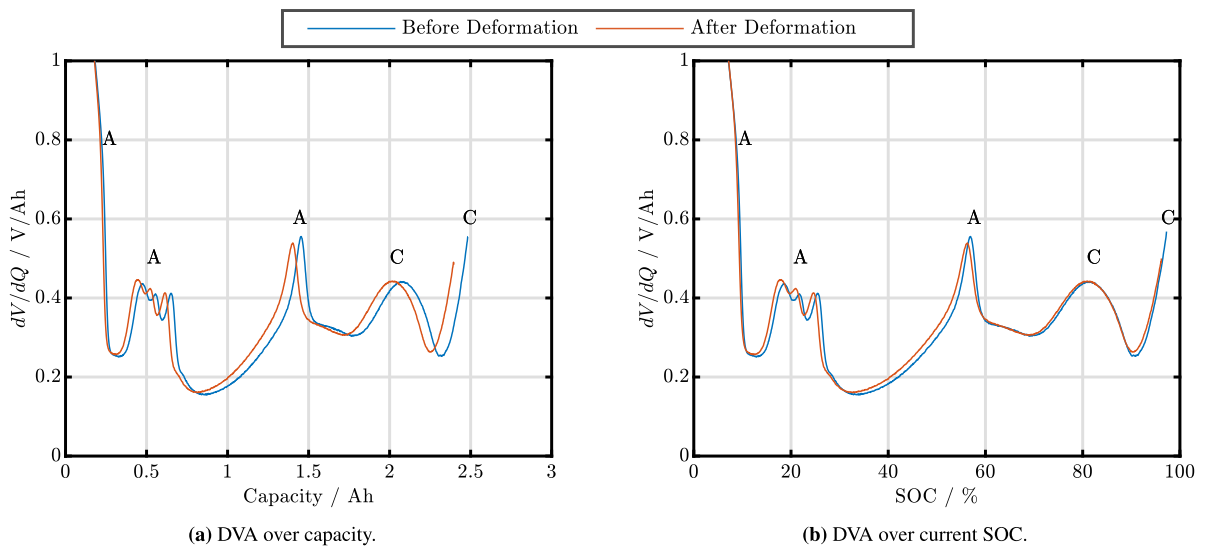


Fig. 8. DVA over capacity and over current SOH for a Samsung INR18650-25R M cell before and after 6mm deformation with a 20mm cylindric impactor. Peaks which are characteristic for the anode (A) and cathode (C) [74] are marked.

other boundary layers [81–83]. OCV measurements and DVA analysis indicated, as opposed to observations in the SEM analysis, that the loss of capacity cannot be attributed mainly to the anode but originates from a global loss of useable material. That is because the characteristic peaks attributed to anode and cathode barely change their relative positions.

All in all, no cell in these test series exhibited a hazardous event and no indication of safety-critical behavior. However, this must not be construed as a guarantee for cell safety under mechanical deformation, as the small sample size of 5 per variation allows no significantly reliable conclusion on the impact of cell safety. Such damage may severely increase the risk of a hazardous event without being trackable in the conducted test series. Additionally, other tests conducted by the authors of this publication have shown that, while 18 650 batteries are very resilient against deformation in the jelly roll area, deformations at the positive pole as small as 1 mm may cause electrolyte leakage and functionality delay or loss of the CID. Also, deformations in the area of the anode and separator overhang may be more critical, as they may establish direct contact between the electrodes. Furthermore, the results are limited to the specific load case and the two tested cell types.

5. Conclusion

In this work, long-term cyclic aging test series with deformed cells of two types of high-power 18 650 cells (with mandrel and mandrel-free) were conducted. In the long-term cyclic aging studies, no hazardous events were observed. The aging test series showed that minor deformations have an insignificant impact on the CC discharge capacity, whereas severe deformations lead to capacity drops directly after deformation but little to no accelerated aging after these initial drops. CT, post-mortem, and SEM analysis indicated significant differences in cell internal stress distribution and local component damaging for the deformed cells, but without causing separator failure.

Further electrical analysis showed significantly increased CC–CV charge capacity in the cycle after mechanical deformation due to prolonged CV phases. The prolonged CV-phases with increased charge capacity and following CC–CV discharge capacity drops and after deformation may offer an approach for detecting mechanical damage. DVA indicated no damage primarily on either anode or cathode but global capacity losses.

While the cells in the conducted investigations exhibited no safety-critical behavior, the small sample size of 5 cells per variation has to be highlighted, which does not allow reliable statistical conclusions. Either way, other deformation scenarios are far more critical, and very high loads may lead to instant thermal runaway, which still needs to be addressed with proper module design.

Future work may investigate much higher sample sizes to draw more statistically reliable conclusions. Also, other cell types, load scenarios (e.g. other impactors, deformation locations, axial compression), and even more severe cell deformations with electrode fractures could be investigated. Furthermore, the investigation of cells with graphite-silicon anodes, which exhibit higher cyclic and irreversible volume expansion, might be relevant to upcoming cell generations. The effect, which leads to increased charge capacity in the cycle after the deformation, might be better understood after further testing with half-cells or chemical analysis in the deformation areas.

CRedit authorship contribution statement

Markus Spielbauer: Conceptualization, Methodology, Validation, Formal analysis, Investigation, Resources, Data curation, Writing – original draft, Writing – review & editing, Visualization. **Jonas Soellner:** Conceptualization, Methodology, Writing – review & editing. **Philipp Berg:** Methodology, Writing – review & editing, Funding acquisition. **Korbinian Koch:** Conceptualization, Methodology, Investigation, Resources, Writing – review & editing. **Peter Keil:** Validation, Formal

analysis, Investigation, Resources, Data curation, Writing – review & editing. **Christian Rosenmüller:** Formal analysis, Investigation, Resources, Writing – review & editing. **Oliver Bohlen:** Conceptualization, Methodology, Resources, Writing – review & editing, Supervision, Project administration, Funding acquisition. **Andreas Jossen:** Conceptualization, Methodology, Resources, Writing – review & editing, Supervision, Project administration, Funding acquisition.

Declaration of competing interest

The authors declare that they have no known competing financial interests or personal relationships that could have appeared to influence the work reported in this paper.

Data availability

The data that has been used is available upon request.

Acknowledgments

Funding from the German Federal Ministry for Economic Affairs and Energy (BMWi) of the project ReVISED Batt [03ETE 004C] and managing by the Projektträger Jülich (PtJ) as well as funding by the The Bavarian Ministry for Science, Research and Culture of the project Safe-Mu-Mob is gratefully acknowledged. The authors also want to thank Dr. Sarah Hartmann and Philip Daubinger from Fraunhofer ISC for conducting SEM scans, Prof. Dr. Gregor Feiertag for supporting this project by granting access to the CT and Robert Stanger, Leonard Janczyk and Varnim Goyal from Hilti Entwicklungsgesellschaft GmbH for fruitful discussions and for providing cells for the test series.

Appendix. Abbreviations

EIS	Electrochemical Impedance Spectroscopy
ISC	Internal Short Circuit
CC	Constant Current
CID	Current Interruptive Device
CT	Computed Tomography
CV	Constant Voltage
DVA	Differential Voltage Analysis
LFP	Lithium Iron Phosphate
OCV	Open Circuit Voltage
SEI	Solid Electrolyte Interphase
SEM	Scanning Electron Microscope
SOC	State of Charge
SOH	State of Health

References

- [1] Q. Wang, P. Ping, X. Zhao, G. Chu, J. Sun, C. Chen, Thermal runaway caused fire and explosion of lithium ion battery, *J. Power Sources* 208 (2012) 210–224, <http://dx.doi.org/10.1016/j.jpowsour.2012.02.038>.
- [2] D. Lisbona, T. Snee, A review of hazards associated with primary lithium and lithium-ion batteries, *Process Safety Environ. Protect.* 89 (6) (2011) 434–442, <http://dx.doi.org/10.1016/j.psep.2011.06.022>.
- [3] C. Hendricks, N. Williard, S. Mathew, M. Pecht, A failure modes, mechanisms, and effects analysis (FMMEA) of lithium-ion batteries, *J. Power Sources* 297 (2015) 113–120, <http://dx.doi.org/10.1016/j.jpowsour.2015.07.100>.
- [4] R. Bubbico, V. Greco, C. Menale, Hazardous scenarios identification for Li-ion secondary batteries, *Saf. Sci.* 108 (2018) 72–88, <http://dx.doi.org/10.1016/j.ssci.2018.04.024>.
- [5] A. Kvasha, C. Gutiérrez, U. Osa, I. de Meatza, J.A. Blazquez, H. Macicior, I. Urdampilleta, A comparative study of thermal runaway of commercial lithium ion cells, *Energy* 159 (2018) 547–557, <http://dx.doi.org/10.1016/j.energy.2018.06.173>.
- [6] R. Xiong, L. Li, J. Tian, Towards a smarter battery management system: A critical review on battery state of health monitoring methods, *J. Power Sources* 405 (2018) 18–29, <http://dx.doi.org/10.1016/j.jpowsour.2018.10.019>.

- [7] W. Waag, C. Fleischer, D.U. Sauer, Critical review of the methods for monitoring of lithium-ion batteries in electric and hybrid vehicles, *J. Power Sources* 258 (2014) 321–339, <http://dx.doi.org/10.1016/j.jpowsour.2014.02.064>.
- [8] Z. Liao, S. Zhang, K. Li, G. Zhang, T.G. Habetler, A survey of methods for monitoring and detecting thermal runaway of lithium-ion batteries, *J. Power Sources* 436 (2019) 226879, <http://dx.doi.org/10.1016/j.jpowsour.2019.226879>.
- [9] D. Sauerteig, S. Ivanov, H. Reinshagen, A. Bund, Reversible and irreversible dilation of lithium-ion battery electrodes investigated by in-situ dilatometry, *J. Power Sources* 342 (2017) 939–946, <http://dx.doi.org/10.1016/j.jpowsour.2016.12.121>.
- [10] D. Sauerteig, N. Hanselmann, A. Arzberger, H. Reinshagen, S. Ivanov, A. Bund, Electrochemical-mechanical coupled modeling and parameterization of swelling and ionic transport in lithium-ion batteries, *J. Power Sources* 378 (2018) 235–247, <http://dx.doi.org/10.1016/j.jpowsour.2017.12.044>.
- [11] J. Park, S. Kalnaus, S. Han, Y.K. Lee, G.B. Less, N.J. Dudney, C. Daniel, A.M. Sastry, In situ atomic force microscopy studies on lithium (de)intercalation-induced morphology changes in Li_xCoO_2 micro-machined thin film electrodes, *J. Power Sources* 222 (2013) 417–425, <http://dx.doi.org/10.1016/j.jpowsour.2012.09.017>.
- [12] J.H. Lee, H.M. Lee, S. Ahn, Battery dimensional changes occurring during charge/discharge cycles—thin rectangular lithium ion and polymer cells, *J. Power Sources* 119–121 (2003) 833–837, [http://dx.doi.org/10.1016/S0378-7753\(03\)00281-7](http://dx.doi.org/10.1016/S0378-7753(03)00281-7).
- [13] J. Vetter, P. Novák, M.R. Wagner, C. Veit, K.-C. Möller, J.O. Besenhard, M. Winter, M. Wohlfahrt-Mehrens, C. Vogler, A. Hammouche, Ageing mechanisms in lithium-ion batteries, *J. Power Sources* 147 (1–2) (2005) 269–281, <http://dx.doi.org/10.1016/j.jpowsour.2005.01.006>.
- [14] M. Petzl, M. Kasper, M.A. Danzer, Lithium plating in a commercial lithium-ion battery – A low-temperature aging study, *J. Power Sources* 275 (2015) 799–807, <http://dx.doi.org/10.1016/j.jpowsour.2014.11.065>.
- [15] J. Luo, C.Y. Dai, Z. Wang, K. Liu, W.G. Mao, D.N. Fang, X. Chen, In-situ measurements of mechanical and volume change of LiCoO_2 lithium-ion batteries during repeated charge–discharge cycling by using digital image correlation, *Measurement* 94 (2016) 759–770, <http://dx.doi.org/10.1016/j.measurement.2016.09.023>.
- [16] J. Cannarella, C.B. Arnold, Stress evolution and capacity fade in constrained lithium-ion pouch cells, *J. Power Sources* 245 (2014) 745–751, <http://dx.doi.org/10.1016/j.jpowsour.2013.06.165>.
- [17] M. Wünsch, J. Kaufman, D.U. Sauer, Investigation of the influence of different bracing of automotive pouch cells on cyclic lifetime and impedance spectra, *J. Energy Storage* 21 (2019) 149–155, <http://dx.doi.org/10.1016/j.est.2018.11.019>.
- [18] H.Y. Tran, G. Greco, C. Täubert, M. Wohlfahrt-Mehrens, W. Haselrieder, A. Kwade, Influence of electrode preparation on the electrochemical performance of $\text{LiNi}_0.8\text{Co}_0.15\text{Al}_0.05\text{O}_2$ composite electrodes for lithium-ion batteries, *J. Power Sources* 210 (2012) 276–285, <http://dx.doi.org/10.1016/j.jpowsour.2012.03.017>.
- [19] V. Müller, R.-G. Scurtu, K. Richter, T. Waldmann, M. Memm, M.A. Danzer, M. Wohlfahrt-Mehrens, Effects of mechanical compression on the aging and the expansion behavior of Si/C-composite|NMC811 in different lithium-ion battery cell formats, *J. Electrochem. Soc.* 166 (15) (2019) A3796–A3805, <http://dx.doi.org/10.1149/2.1121915jes>.
- [20] V. Müller, R.-G. Scurtu, M. Memm, M.A. Danzer, M. Wohlfahrt-Mehrens, Study of the influence of mechanical pressure on the performance and aging of lithium-ion battery cells, *J. Power Sources* 440 (2019) 227148, <http://dx.doi.org/10.1016/j.jpowsour.2019.227148>.
- [21] A. Pfrang, A. Kersys, A. Kriston, D.U. Sauer, C. Rahe, S. Käbitz, E. Figgemeier, Geometrical inhomogeneities as cause of mechanical failure in commercial 18650 lithium ion cells, *J. Electrochem. Soc.* 166 (15) (2019) A3745–A3752, <http://dx.doi.org/10.1149/2.0551914jes>.
- [22] L. Willenberg, P. Dechent, G. Fuchs, M. Teuber, M. Eckert, M. Graff, N. Kürten, D.U. Sauer, E. Figgemeier, The development of jelly roll deformation in 18650 lithium-ion batteries at low state of charge, *J. Electrochem. Soc.* 167 (12) (2020) 120502, <http://dx.doi.org/10.1149/1945-7111/aba96d>.
- [23] T.C. Bach, S.F. Schuster, E. Fleder, J. Müller, M.J. Brand, H. Lormann, A. Jossen, G. Sextl, Nonlinear aging of cylindrical lithium-ion cells linked to heterogeneous compression, *J. Energy Storage* 5 (2016) 212–223, <http://dx.doi.org/10.1016/j.est.2016.01.003>.
- [24] Q. Liu, C. Du, B. Shen, P. Zuo, X. Cheng, Y. Ma, G. Yin, Y. Gao, Understanding undesirable anode lithium plating issues in lithium-ion batteries, *RSC Adv.* 6 (91) (2016) 88683–88700, <http://dx.doi.org/10.1039/C6RA19482F>.
- [25] M.F. Lagadic, R. Zahn, V. Wood, Designing polyolefin separators to minimize the impact of local compressive stresses on lithium ion battery performance, *J. Electrochem. Soc.* 165 (9) (2018) A1829–A1836.
- [26] X.M. Liu, A. Fang, M.P. Haataja, A. C.B., Size dependence of transport non-uniformities on localized plating in lithium-ion batteries, *J. Electrochem. Soc.* 5 (165) (2018) A1147–A1155.
- [27] G. Fuchs, L. Willenberg, F. Ringbeck, D.U. Sauer, Post-mortem analysis of inhomogeneous induced pressure on commercial lithium-ion pouch cells and their effects, *Sustainability* 11 (23) (2019) 6738, <http://dx.doi.org/10.3390/su11236738>.
- [28] P. Daubinger, F. Ebert, S. Hartmann, G.A. Giffin, Impact of electrochemical and mechanical interactions on lithium-ion battery performance investigated by operando dilatometry, *J. Power Sources* 488 (2021) 229457, <http://dx.doi.org/10.1016/j.jpowsour.2021.229457>.
- [29] X. Gao, P. He, J. Ren, J. Xu, Modeling of contact stress among compound particles in high energy lithium-ion battery, *Energy Storage Mater.* 18 (2019) 23–33, <http://dx.doi.org/10.1016/j.ensm.2019.02.007>.
- [30] F. Hao, X. Gao, D. Fang, Diffusion-induced stresses of electrode nanomaterials in lithium-ion battery: The effects of surface stress, *J. Appl. Phys.* 112 (10) (2012) 103507, <http://dx.doi.org/10.1063/1.4767913>.
- [31] S. Huang, F. Fan, J. Li, S. Zhang, T. Zhu, Stress generation during lithiation of high-capacity electrode particles in lithium ion batteries, *Acta Mater.* 61 (12) (2013) 4354–4364, <http://dx.doi.org/10.1016/j.actamat.2013.04.007>.
- [32] F.M. Kindermann, A. Noel, S.V. Erhard, A. Jossen, Long-term equalization effects in li-ion batteries due to local state of charge inhomogeneities and their impact on impedance measurements, *Electrochim. Acta* 185 (2015) 107–116, <http://dx.doi.org/10.1016/j.electacta.2015.10.108>.
- [33] M.N. Obrovac, L. Christensen, D.B. Le, J.R. Dahn, Alloy design for lithium-ion battery anodes, *J. Electrochem. Soc.* 154 (9) (2007) A849–A855.
- [34] C.K. Chan, H. Peng, G. Liu, K. McIlwrath, X.F. Zhang, R.A. Huggins, Y. Cui, High-performance lithium battery anodes using silicon nanowires, *Nature Nanotechnol.* 3 (1) (2008) 31–35, <http://dx.doi.org/10.1038/nnano.2007.411>.
- [35] E. Sahraei, J. Meier, T. Wierzbicki, Characterizing and modeling mechanical properties and onset of short circuit for three types of lithium-ion pouch cells, *J. Power Sources* 247 (2014) 503–516, <http://dx.doi.org/10.1016/j.jpowsour.2013.08.056>.
- [36] J. Zhu, X. Zhang, E. Sahraei, T. Wierzbicki, Deformation and failure mechanisms of 18650 battery cells under axial compression, *J. Power Sources* 336 (2016) 332–340, <http://dx.doi.org/10.1016/j.jpowsour.2016.10.064>.
- [37] L. Wang, S. Yin, J. Xu, A detailed computational model for cylindrical lithium-ion batteries under mechanical loading: From cell deformation to short-circuit onset, *J. Power Sources* 413 (2019) 284–292, <http://dx.doi.org/10.1016/j.jpowsour.2018.12.059>.
- [38] F. Ren, T. Cox, H. Wang, Thermal runaway risk evaluation of Li-ion cells using a pinch–torsion test, *J. Power Sources* 249 (2014) 156–162, <http://dx.doi.org/10.1016/j.jpowsour.2013.10.058>.
- [39] I. Avdeev, M. Gilaki, Structural analysis and experimental characterization of cylindrical lithium-ion battery cells subject to lateral impact, *J. Power Sources* 271 (2014) 382–391, <http://dx.doi.org/10.1016/j.jpowsour.2014.08.014>.
- [40] B. Mao, H. Chen, Z. Cui, T. Wu, Q. Wang, Failure mechanism of the lithium ion battery during nail penetration, *Int. J. Heat Mass Transfer* 122 (2018) 1103–1115, <http://dx.doi.org/10.1016/j.ijheatmasstransfer.2018.02.036>.
- [41] J. Zhu, T. Wierzbicki, W. Li, A review of safety-focused mechanical modeling of commercial lithium-ion batteries, *J. Power Sources* 378 (2018) 153–168, <http://dx.doi.org/10.1016/j.jpowsour.2017.12.034>.
- [42] B. Liu, Y. Jia, C. Yuan, L. Wang, X. Gao, S. Yin, J. Xu, Safety issues and mechanisms of lithium-ion battery cell upon mechanical abusive loading: A review, *Energy Storage Mater.* 24 (2020) 85–112, <http://dx.doi.org/10.1016/j.ensm.2019.06.036>.
- [43] J. Xu, B. Liu, X. Wang, D. Hu, Computational model of 18650 lithium-ion battery with coupled strain rate and SOC dependencies, *Appl. Energy* 172 (2016) 180–189, <http://dx.doi.org/10.1016/j.apenergy.2016.03.108>.
- [44] J. Xu, Y. Jia, B. Liu, H. Zhao, H. Yu, J. Li, S. Yin, Coupling effect of state-of-health and state-of-charge on the mechanical integrity of lithium-ion batteries, *Exp. Mech.* 58 (4) (2018) 633–643, <http://dx.doi.org/10.1007/s11340-018-0380-9>.
- [45] Y. Jia, S. Yin, B. Liu, H. Zhao, H. Yu, J. Li, J. Xu, Unlocking the coupling mechanical-electrochemical behavior of lithium-ion battery upon dynamic mechanical loading, *Energy* 166 (2019) 951–960, <http://dx.doi.org/10.1016/j.energy.2018.10.142>.
- [46] C. Peabody, C.B. Arnold, The role of mechanically induced separator creep in lithium-ion battery capacity fade, *J. Power Sources* 196 (19) (2011) 8147–8153, <http://dx.doi.org/10.1016/j.jpowsour.2011.05.023>.
- [47] M.J. Brand, M.H. Hofmann, M. Steinhardt, S.F. Schuster, A. Jossen, Current distribution within parallel-connected battery cells, *J. Power Sources* 334 (2016) 202–212, <http://dx.doi.org/10.1016/j.jpowsour.2016.10.010>.
- [48] M.H. Hofmann, K. Czyrka, M.J. Brand, M. Steinhardt, A. Noel, F.B. Spingler, A. Jossen, Dynamics of current distribution within battery cells connected in parallel, *J. Energy Storage* 20 (2) (2018) 120–133, <http://dx.doi.org/10.1016/j.est.2018.08.013>.
- [49] Y. Xia, T. Wierzbicki, E. Sahraei, X. Zhang, Damage of cells and battery packs due to ground impact, *J. Power Sources* 267 (2014) 78–97, <http://dx.doi.org/10.1016/j.jpowsour.2014.05.078>.
- [50] P. Keil, A. Jossen, Impact of dynamic driving loads and regenerative braking on the aging of lithium-ion batteries in electric vehicles, *J. Electrochem. Soc.* 164 (13) (2017) A3081–A3092, <http://dx.doi.org/10.1149/2.0801713jes>.
- [51] S.F. Schuster, T. Bach, E. Fleder, J. Müller, M. Brand, G. Sextl, A. Jossen, Nonlinear aging characteristics of lithium-ion cells under different operational conditions, *J. Energy Storage* 1 (2015) 44–53, <http://dx.doi.org/10.1016/j.est.2015.05.003>.

- [52] M. Ecker, N. Nieto, S. Käbitz, J. Schmalstieg, H. Blanke, A. Warnecke, D.U. Sauer, Calendar and cycle life study of Li(NiMnCo)O₂-based 18650 lithium-ion batteries, *J. Power Sources* 248 (2014) 839–851, <http://dx.doi.org/10.1016/j.jpowsour.2013.09.143>.
- [53] A. Yang, Y. Wang, F. Yang, D. Wang, Y. Zi, K.L. Tsui, B. Zhang, A comprehensive investigation of lithium-ion battery degradation performance at different discharge rates, *J. Power Sources* 443 (1–2) (2019) 227108, <http://dx.doi.org/10.1016/j.jpowsour.2019.227108>.
- [54] J.Y. Kim, K.T. Yoo, D.O. Kim, M.H. Lee, W.J. Yang, J.W. Byeon, Evaluation of health and safety of mechanically fatigued rechargeable lithium polymer batteries for flexible electronics applications, *Microelectron. Reliab.* 100–101 (2019) 113441, <http://dx.doi.org/10.1016/j.microrel.2019.113441>.
- [55] X. Zhu, H. Wang, S. Allu, Y. Gao, E. Cakmak, E.J. Hopkins, G.M. Veith, Z. Wang, Investigation on capacity loss mechanisms of lithium-ion pouch cells under mechanical indentation conditions, *J. Power Sources* 465 (2020) 228314, <http://dx.doi.org/10.1016/j.jpowsour.2020.228314>.
- [56] J.K.S. Goodman, J.T. Miller, S. Kreuzer, J. Forman, S. Wi, J.-m. Choi, B. Oh, K. White, Lithium-ion cell response to mechanical abuse: Three-point bend, *J. Energy Storage* 28 (Issues 3–4) (2020) 101244, <http://dx.doi.org/10.1016/j.est.2020.101244>.
- [57] W. Shuai, E. Li, H. Wang, An equivalent circuit model of a deformed Li-ion battery with parameter identification, *Int. J. Energy Res.* 44 (11) (2020) 8372–8387, <http://dx.doi.org/10.1002/er.5500>.
- [58] E. Sahraei, M. Gilaki, W. Lynch, J. Kirtley, D. Soudbakhsh, Cycling results of mechanically damaged li-ion batteries, in: 2019 IEEE Electric Ship Technologies Symposium (ESTS), 2019, pp. 226–230, <http://dx.doi.org/10.1109/ESTS.2019.8847923>.
- [59] D. Soudbakhsh, M. Gilaki, W. Lynch, P. Zhang, T. Choi, E. Sahraei, Electrical response of mechanically damaged lithium-ion batteries, *Energies* 13 (17) (2020) 4284, <http://dx.doi.org/10.3390/en13174284>.
- [60] L. Li, X. Chen, Q. Yuan, T. Wang, H. Ji, S. Papović, K. Raleva, F. Pan, T. Yang, J. Li, Effects of minor mechanical deformation on the lifetime and performance of commercial 21700 lithium-ion battery, *J. Electrochem. Soc.* 169 (6) (2022) 060544, <http://dx.doi.org/10.1149/1945-7111/ac79d4>.
- [61] Samsung, INR18650-25r data sheet, 2014.
- [62] Sony, US18650VTC5 Data Sheet.
- [63] I. Zilberman, S. Ludwig, A. Jossen, Cell-to-cell variation of calendar aging and reversible self-discharge in 18650 nickel-rich, silicon-graphite lithium-ion cells, *J. Energy Storage* 26 (2019) 100900, <http://dx.doi.org/10.1016/j.est.2019.100900>.
- [64] B. Epding, B. Rumberg, H. Jahnke, I. Stradtman, A. Kwade, Investigation of significant capacity recovery effects due to long rest periods during high current cyclic aging tests in automotive lithium ion cells and their influence on lifetime, *J. Energy Storage* 22 (1–2) (2019) 249–256, <http://dx.doi.org/10.1016/j.est.2019.02.015>.
- [65] N.K. Thangavel, S. Mundhe, M.M. Islam, G. Newaz, L.M.R. Arava, Probing of internal short circuit in lithium-ion pouch cells by electrochemical impedance spectroscopy under mechanical abusive conditions, *J. Electrochem. Soc.* 167 (16) (2020) 160553, <http://dx.doi.org/10.1149/1945-7111/abd452>.
- [66] I. Bloom, A.N. Jansen, D.P. Abraham, J. Knuth, S.A. Jones, V.S. Battaglia, G.L. Henriksen, Differential voltage analyses of high-power, lithium-ion cells, *J. Power Sources* 139 (1–2) (2005) 295–303, <http://dx.doi.org/10.1016/j.jpowsour.2004.07.021>.
- [67] M. Dubarry, V. Svoboda, R. Hwu, B. Yann Liaw, Incremental capacity analysis and close-to-equilibrium OCV measurements to quantify capacity fade in commercial rechargeable lithium batteries, *Electrochem. Solid-State Lett.* 9 (10) (2006) A454, <http://dx.doi.org/10.1149/1.2221767>.
- [68] D.-I. Stroe, E. Schaltz, Lithium-ion battery state-of-health estimation using the incremental capacity analysis technique, *IEEE Trans. Ind. Appl.* 56 (1) (2020) 678–685, <http://dx.doi.org/10.1109/TIA.2019.2955396>.
- [69] J.P. Schmidt, Verfahren zur Charakterisierung und Modellierung von Lithium-Ionen Zellen (Ph.D. thesis), Karlsruhe Institut für Technologie, 2013.
- [70] J.P. Fath, D. Dragicevic, L. Bittel, A. Nuhic, J. Sieg, S. Hahn, L. Alsheimer, B. Spier, T. Wetzel, Quantification of aging mechanisms and inhomogeneity in cycled lithium-ion cells by differential voltage analysis, *J. Energy Storage* 25 (2019) 100813, <http://dx.doi.org/10.1016/j.est.2019.100813>.
- [71] T. Waldmann, M. Wilka, M. Kasper, M. Fleischhammer, M. Wohlfahrt-Mehrens, Temperature dependent ageing mechanisms in lithium-ion batteries – A post-mortem study, *J. Power Sources* 262 (2014) 129–135, <http://dx.doi.org/10.1016/j.jpowsour.2014.03.112>.
- [72] R. Carter, E.J. Klein, R.W. Atkinson, C.T. Love, Mechanical collapse as primary degradation mode in mandrel-free 18650 li-ion cells operated at 0 °C, *J. Power Sources* 437 (2019) 226820, <http://dx.doi.org/10.1016/j.jpowsour.2019.226820>.
- [73] A. Pfrang, A. Kersys, A. Kriston, D.U. Sauer, C. Rahe, S. Käbitz, E. Figgemeier, Long-term cycling induced jelly roll deformation in commercial 18650 cells, *J. Power Sources* 392 (9) (2018) 168–175, <http://dx.doi.org/10.1016/j.jpowsour.2018.03.065>.
- [74] P. Keil, S. Schuster, J. Wilhelm, J. Travi, A. Hauser, R. Karl, A. Jossen, Calendar aging of lithium-ion batteries I. Impact of the graphite anode on capacity fade, *J. Electrochem. Soc.* 163 (9) (2016) A1872–A1880.
- [75] H. Luo, J. Zhu, E. Sahraei, Y. Xia, Adhesion strength of the cathode in lithium-ion batteries under combined tension/shear loadings, *RSC Adv.* 8 (8) (2018) 3996–4005, <http://dx.doi.org/10.1039/C7RA12382E>.
- [76] M. Gilaki, I. Avdeev, Impact modeling of cylindrical lithium-ion battery cells: a heterogeneous approach, *J. Power Sources* 328 (2) (2016) 443–451, <http://dx.doi.org/10.1016/j.jpowsour.2016.08.034>.
- [77] L. Zhang, Z. Ning, H. Peng, Z. Mu, C. Sun, Effects of vibration on the electrical performance of lithium-ion cells based on mathematical statistics, *Appl. Sci.* 7 (8) (2017) 802, <http://dx.doi.org/10.3390/app7080802>.
- [78] K. Fink, S. Santhanagopalan, J. Hartig, L. Cao, Characterization of aged li-ion battery components for direct recycling process design, *J. Electrochem. Soc.* 166 (15) (2019) A3775–A3783.
- [79] H. Ou, H. Peng, L. Shi, U. Ismat, W. Zhang, X. Zhang, Investigation on the blanking properties of thin multi-layer electrode of lithium-ion battery, *J. Phys. Chem. Solids* 134 (2019) 14–20, <http://dx.doi.org/10.1016/j.jpcs.2019.05.033>.
- [80] Y. Ji, X. Chen, T. Wang, H. Ji, Y. Zhang, Q. Yuan, L. Li, Coupled effects of charge–discharge cycles and rates on the mechanical behavior of electrodes in lithium-ion batteries, *J. Energy Storage* 30 (13) (2020) 101577, <http://dx.doi.org/10.1016/j.est.2020.101577>.
- [81] F.-M. Wang, M.-H. Yu, Y.-J. Hsiao, Y. Tsai, B.-J. Hwang, Y.-Y. Wang, C.-C. Wan, Aging effects to solid electrolyte interface (SEI) membrane formation and the performance analysis of lithium ion batteries, *Int. J. Electrochem. Sci.* 6 (4) (2011) 1014–1026.
- [82] D. Liu, Y. Wang, Y. Xie, L. He, J. Chen, K. Wu, R. Xu, Y. Gao, On the stress characteristics of graphite anode in commercial pouch lithium-ion battery, *J. Power Sources* 232 (25) (2013) 29–33, <http://dx.doi.org/10.1016/j.jpowsour.2012.12.110>.
- [83] I. Laresgoiti, S. Käbitz, M. Ecker, D.U. Sauer, Modeling mechanical degradation in lithium ion batteries during cycling: Solid electrolyte interphase fracture, *J. Power Sources* 300 (2015) 112–122, <http://dx.doi.org/10.1016/j.jpowsour.2015.09.033>.